The International Journal of Advanced Manufacturing Technology
https://doi.org/10.1007/s00170-018-2678-2

ORIGINAL ARTICLE

Finite element simulation of high speed micro milling in the presence of tool run-out with experimental validations

Aldo Attanasio[1] · Andrea Abeni[1] · Tuğrul Özel[2] · Elisabetta Ceretti[1]

Received: 13 May 2018 / Accepted: 7 September 2018

Abstract
Micro milling process of CuZn37 brass is considered important due to applications in tool production for micro moulding and micro replication technology. The variations in material properties, work material adhesion to tool surfaces, burr formation, and tool wear result in loss of productivity. The deformed chip shapes together with localized temperature, plastic strain, and cutting forces during micro milling process can be predicted using finite element (FE) modeling and simulation. However, tool-workpiece engagement suffers from tool run-out affecting process performance in surface generation. This work provides experimental investigations on effects of tool run-out as well as process insight obtained from simulation of chip flow, with and without considering tool run-out. Scanning electron microscope (SEM) observation of the 3D chip shapes demonstrates ductile deformed surfaces together with localized serration behavior. FE simulations are utilized to investigate the effects of micro milling operation, cutting speed, and feed rate on forces, chip flow, and shapes. Predicted cutting forces and chip flow results from simulations are compared with force measurements, tool run-out, and chip morphology revealing reasonable agreements.

Keywords Micro machining · Finite element method (FEM) · Force

1 Introduction

The demand for miniaturized end-products has been continuously increasing in biomedical, automotive, aerospace, and electronics industries [1]. Among different processes commonly used to produce these products, micro turning and micro milling provide high flexibility, high accuracy, and economic efficiency due to high material removal rates, low set-up costs, and low material waste [2–4]. Micro milling is among the most versatile machining processes that allow wide spread of miniature components possessing micrometric dimensions. The most successful application of this technology is certainly in the dies and moulds industry for fabrication of tooling to be used in micro moulding and micro replication processes, due to viability of high accuracy geometric dimensions and superior surface finishes at a rather low production cost.

On the other hand, as in macro scale processes [5], the performance of micro milling is affected by a large number of factors and technical issues. In the recent decades, a large number of publications are dedicated to understand micro milling processes. These are mainly concerned with miniature machine tool development, process modeling to achieve a greater understanding about cutting force generation and mechanistic modeling [6–9], chatter vibrations [10], workpiece defects and surface quality, tool edge effects [11], tool run-out effects [12, 13], thermal stability [14], and many other issues. Last several years, researchers also dealt with the possibility of implementing predictive process models with finite element (FE) simulations [13, 15–18], a useful capability to refine the knowledge about force generation and chip formation in micro milling.

In micro milling, tool diameters are typically smaller than 1 mm, tool edge roundness is about a few micrometres, and the chip thickness has the same order of magnitude with edge roundness [19]. At this length scale, ploughing, size effect, burr formation, rapid tool wear, higher than expected cutting forces, and tool run-out cannot be neglected being the most common micro milling related issues [3, 20–22].

✉ Aldo Attanasio
aldo.attanasio@unibs.it

[1] Department of Mechanical and Industrial Engineering, University of Brescia, V. Branze 38, 25123 Brescia, Italy

[2] Industrial and Systems Engineering, Rutgers University, Piscataway, NJ, USA

Published online: 20 September 2018

Among all of these issues in micro milling process, tool run-out is certainly the most important issue causing geometrical inaccuracies, workpiece defects, and burr formation and deserves more attention [12, 13, 20, 21, 23]. This phenomenon occurs due to the sum of the geometrical displacements of the tool axis, the spindle axis, and the tool-holder axis from the ideal axis of rotation [12]. The ratio between this offset and the feed per tooth could be easily high in high speed micro milling (typically rotational speeds that are higher than 10,000 rev/min and up to 100,000 rev/min). The deviation of the tool edge trajectories involves an asymmetric cutting condition. A change of undeformed chip thickness, a load imbalance between the flutes, a decrease of the tool life, and a reduction in workpiece quality are the main consequences of tool run-out.

The development of a good model for describing cutting operation on a micro scale is essential to understand how all process variables influence the final product quality. In fact, the traditional experimental approach runs into several difficulties at this scale. Measuring tool temperature and tool wear, evaluating chip morphology, and determining the cutting force values are challenging tasks. Finite element (FE) simulations can be applied to predict these process variables reasonably well, to analyze the generated surfaces and to optimize the machining parameters.

The main objective of this research was to develop and validate a FE model for simulating micro milling process of lead free brass due to the lack of publications available on this relevant topic. Secondly, the aims were to develop a new procedure to define tool run-out parameters based on experimental testing, Kronenberg cutting force model [24], and to develop FE simulation of micro milling in the presence of tool run-out.

To reach the pursued objectives, experimental tests consisting of micro milling operations under orthogonal conditions were performed. Orthogonal milling configuration was obtained by cutting a thin wall brass structure with an end mill with a helix angle equal to zero (Fig. 1). In this configuration, the total force can be represented in a plane (2D cutting) by two components (i.e., thrust and cutting force components or Fx and Fy components in an XY coordinate system). Moreover, a complete 3D FE model for orthogonal milling was presented. Material behavior in high deformation rate, hardening, and thermal softening is considered even though the thermal softening could be neglected due to the low temperature involved during the micro cutting operation. Cutting forces and chip morphology obtained from FE simulations were compared with experimental results for model validation. Micro milling tests were properly designed to obtain an orthogonal cutting configuration and to allow the comparison with FE simulation predictions. It should be noted that the force measurement system has been tested for accuracy on the load cell to ensure its validity for the desired bandwidth [23].

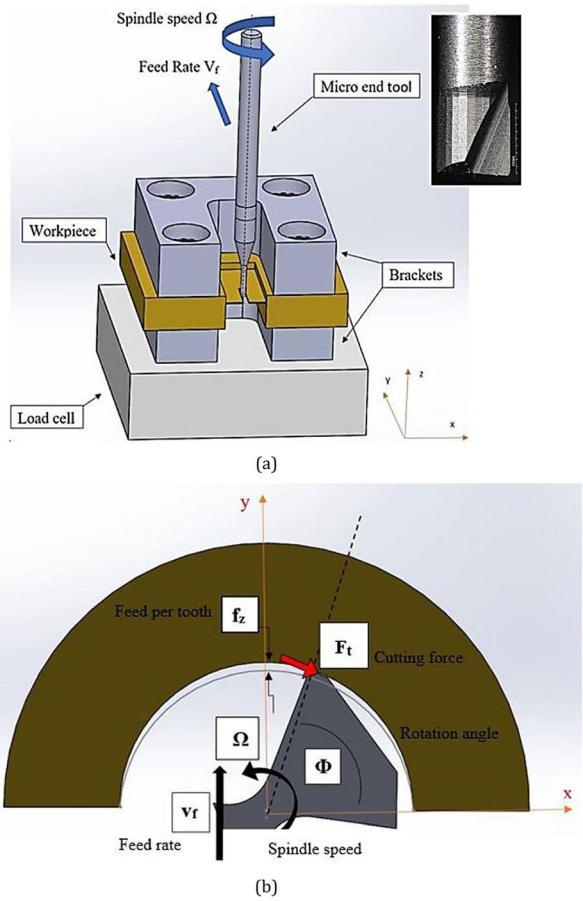

Fig. 1 **a** Orthogonal milling process in 3D configuration. **b** 2D configuration of cutting with a zero helix angle micro end mill

2 Experimental approach

Full immersion micro milling of brass (CuZn37) was performed by using the nano-precision 5-axis machining center Kern Pyramid Nano (± 0.3 μm precision). The experimental setup together with tool and workpiece geometries, positioning, and movements is illustrated in Fig. 1. A prismatic workpiece (30 mm × 26 mm × 5 mm) was blocked between two aluminum brackets and fixed on a three-component load cell (Kistler 9317C) with four bolts. Two machining operations were executed: (i) roughing to prepare a thin wall on the workpiece and (ii) orthogonal milling of the thin walled workpiece. After roughing, the workpiece was heat-treated for stress relief. FE simulations were only concerned with the second operation. A workpiece with 144 μm ± 6 μm thin wall was obtained by using four-flute and 6-mm diameter end mills. Two-flute micro end mills with a rake angle of $\gamma = 0°$ and a helix angle of $\beta = 0°$ from SECO company (103L008R005-MEGA-64-T) were used to cut the thin wall without engaging the tool bottom under dry cutting conditions. The tool material was tungsten carbide (WC/Co) with (Ti,Al)N coating. Tool geometrical details were measured using 3D digital optical microscope Hirox RH-2000

(measurement accuracy of 0.8 μm). The tool diameter was measured as ∅ = 782 μm ± 4 μm and tool edge radius was measured as r_β = 4.7 μm ± 0.4 μm. Only the side cutting edge of the tool was engaged with the workpiece. The cutting conditions allowed this machining process to be considered approximately as orthogonal cutting.

Different cutting speeds were used with the aim of investigating their influence on tool run-out and cutting force values. A new tool was used for each test to avoid tool wear effects. Tool advance per rotation in *x*-direction was kept equal to 10 μm/tooth. The process parameters are summarized in Table 1. During machining, some chip samples were collected and then investigated using a scanning electron microscope (SEM).

A force measurement and data acquisition system that consists of a piezoelectric 3-component force sensor (Kistler 9317C) connected to charge amplifiers (Kistler 5015A) which receives three charge signals proportional to the cutting force as input and returns amplified voltage signals as output was used. This force measuring system accuracy is approximately equal to 0.1 N [12] which is sufficient for capturing forces in micro milling.

In micro milling processes, force signals oscillate of a few Newtons in few milliseconds to overcome the very small feed rate so to maintain adequate productivity [23]. High sampling rates are necessary to avoid aliasing distortions. In this work, the maximum tooth passing frequency was 1 kHz (as indicated in Table 1) and the sampling rate was fixed at 50 kHz. It is a good trade-off between acceptable data size and acquisition quality. Furthermore, a limited bandwidth could distort the force signals, as discussed in references [20, 21, 23]. When tooth passing frequencies overlap the load cell natural frequencies, the ideal condition of unity gain and low phase delay is not guaranteed. The modal parameters of the clamping system (load cell fixed on machining center, workpiece, and brackets) were detected using impact testing by measuring the output forces in each direction. Firstly, only the load cell was hit three times in order to validate the procedure. The natural frequency was experimentally determined (average values Fx 5156 Hz, Fy 4991 Hz) and compared with the value declared by Kistler (5000 Hz), finding a good matching.

Table 1 Micro milling process parameters

Cutting parameters	Test 1	Test 2	Test 3
Cutting speed, v_c [m/min]	50	62.5	75
Tooth passing frequency [Hz]	664	848	1000
Axial depth of cut, a_p [μm]	139	150	143

In Fig. 2a, the frequency response function (FRF) shows the peak around the natural frequency of the load cell. Subsequently, the entire system was tested with the same methodology. The frequency response of the force sensing system is influenced by the stiffness and the mass of each component. The measured natural frequencies of the clamping system decrease from 5000 Hz (i.e., the natural frequency of the load cell) to 2145 Hz for *x*- and 2192 Hz for *y*-directions (Fig. 2b). A smaller bandwidth is the result of the dominant mode decrease, but it remains larger than maximum tooth passing frequency of 1 kHz.

Figure 3 reports the measured cutting forces for each cutting condition. Lower and upper bounds of experimental charts are built with a confidence level equal to 68%. The high scattering of cutting force of test 3 together with the higher values with respect to test 1 and test 2 can be related to the experimental set-up. The thin-wall cut with a higher cutting speed undergoes to greater vibrations which strongly affect the force measurements.

3 Finite element model

In literature, there are several 2D and 3D finite element simulation models reported for the micro milling process. A majority of the 3D FE simulation work considers workpiece as

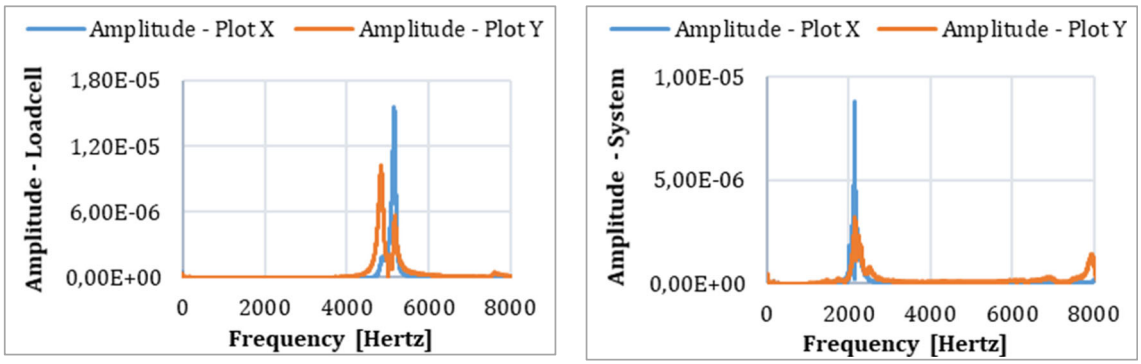

Fig. 2 FRF analysis of natural frequency tested on **a** the load cell and **b** the entire system

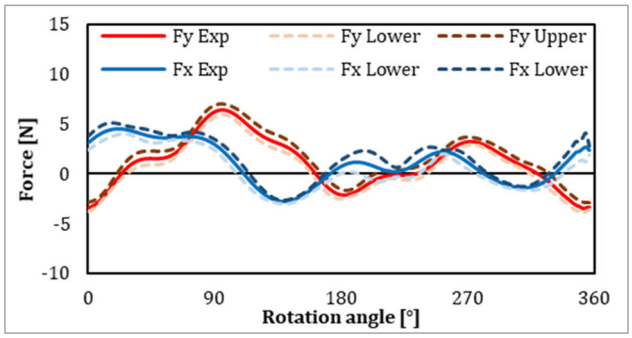

(a)

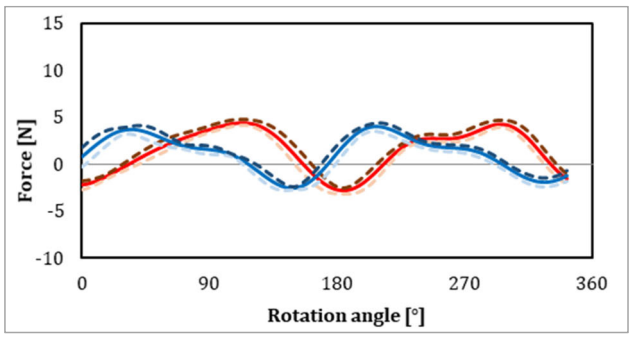

(b)

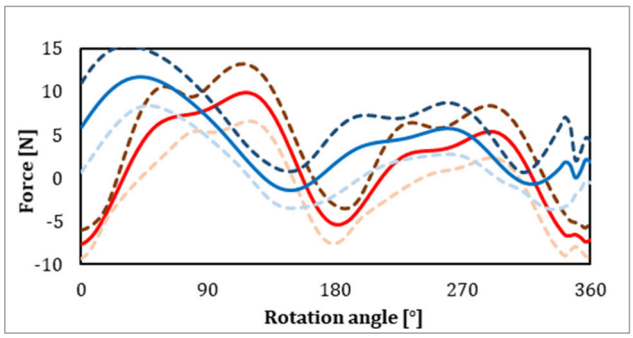

(c)

Fig. 3 Measured cutting forces: **a** test 1, **b** test 2, and **c** test 3

visco-plastic with continuous chip formation [13, 15, 17, 18], but only few publications studied 2D elastic-visco-plastic workpiece deformations and serrated chip formation in micro milling process [16] due to the computational limitations. The difficulty arises in elastic-visco-plastic FE simulation models for 3D micro milling process when simulations do not converge with high-solution accuracy. Therefore, in this study, FE simulations of micro milling were developed by using the visco-plastic workpiece assumption and performing a thermo-mechanical analysis in DEFORM-3D software. A finite element model in 3D was developed instead of a 2D model to capture the 3D chip formation and a more accurate representation of the micro milling process in the simulation results.

FE simulations of micro milling are divided into two groups: (i) FE simulations without considering tool run-out and (ii) FE simulations with considering tool run-out. For each experimental condition, both configurations have been modeled and simulated using DEFORM-3D. The tool run-out offset was created in the tool-workpiece engagement by adjusting the rotation and x, y, z offset settings in the FEM simulations simultaneously so that the simulation model exactly represents the cutting tool edge and the workpiece engagement in the presence of tool run-out.

All of the FE simulations include 3D workpiece geometry with visco-plastic deformable material assumption and a 3D micro milling tool geometry as rigid body. Figure 4a shows the simulation set-up as summarized below. FE simulation begins when tool cutting edge is in contact with the workpiece, assuming an initial cutting force equal to zero and a temperature of 20 °C. Between two consecutive steps, a time increment of 5E-07 s has been set. At the beginning of the simulation, workpiece mesh has about 44,000 tetrahedral elements. This number was increased up to 200,000 to ensure a high-quality mesh during FE simulations. A minimum element size was kept constant as 1.3 μm. The highest mesh density region was placed around the tool-workpiece contact zone and allowed to follow the chip developed by the milling process. The heat generated by the workpiece deformation was allowed to transfer along the tool path surface and the lateral surfaces. The external surface temperature was fixed at 20 °C. Some boundary nodes were fixed in the three directions as shown in Fig. 4a (red nodes), but surfaces perpendicular to the z-axis were allowed to move in order to examine the workpiece deformation also in z-direction. Figure 4b shows the configuration considered with tool run-out and Fig. 4c shows a typical cutting force plot for one full period when two flutes are engaged with the workpiece indicating the run-out effect on the cutting force.

The tool geometry, designed by using a CAD model, was meshed into 210,000 tetrahedral elements with a minimum size of 0.8 μm, concentrated around the active tool cutting edge.

For FE simulations with negligible tool run-out, only one flute cutting was modeled. In the case with considerable tool run-out, cutting with both flutes was simulated in order to underline the differences related to cutting forces and chip morphology between the first and the second edge cut. In particular, for each tool flute cutting, a simulation was designed changing workpiece geometry and tool movement details by considering tool run-out effects.

The CuZn37 material constitutive model was implemented by using Johnson-Cook [25] law. The flow stress is defined as shown in Eq. (1):

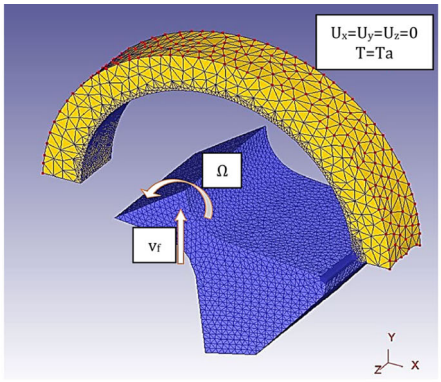

(a)

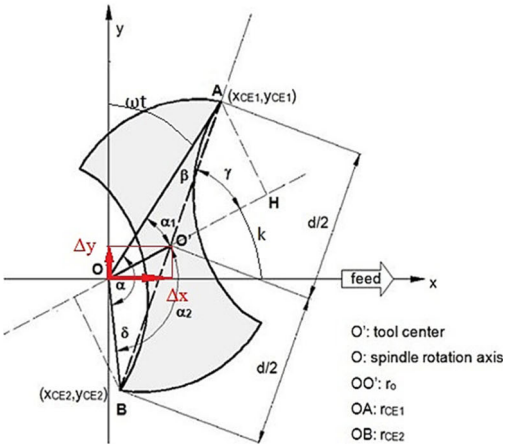

(b)

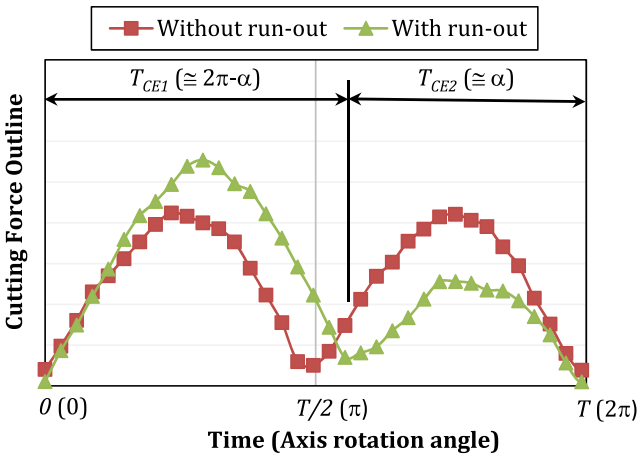

(c)

Fig. 4 Micro milling: **(a)** FEM 3D model with boundary conditions; **(b)** configuration with tool run-out; **(c)** outline curves of cutting force for a two-flute micro end mill without and with tool run-out

$$\sigma = [A + B\varepsilon^{n}]\left[1 + Cln\frac{\dot{\varepsilon}}{\dot{\varepsilon}_0}\right]\left[1-\left(\frac{T-T_0}{T_m-T_0}\right)^{m}\right] \quad (1)$$

where σ is the flow stress, ε is the true strain, $\dot{\varepsilon}$ is the true strain rate, $\dot{\varepsilon}_0$ is the reference true strain rate, T is the work temperature, T_m is the material melting temperature (T_m = 916 °C), and T_0 is the room temperature (T_0 = 20 °C). This model defines the combined contribution of hardening, strain rate, and temperature on the material behavior. Due to the low temperature reached in micro milling, the thermal softening term has a little influence; nevertheless, in this study, it was also considered. The J-C model constants are shown in Table 2.

In each case, workpiece geometry was designed as a half-ring (external diameter = 1000 μm) with a depth in z-direction of 139 μm for test 1, 150 μm for test 2, and 143 μm for test 3, respectively, as measured in experimental tests (see Table 1). The arch-shaped curve represents the undeformed geometry as a result of the previous cut. It was designed using equation set Eq. (2) (Table 3) for micro milling simulations without tool run-out and equation set Eq. (3) (Table 3) for micro milling simulations with tool run-out [7].

The equation set Eq. (3) shall contain some terms in addition to the equation set Eq. (2) in order to consider tool run-out. In Fig. 4b, the problem geometry is shown. The symbols r_{CE1} and r_{CE2} are the radii of the first (A) and the second (B) cutting edge and they are equal to the distance between the tool edges (A and B) and the spindle center (O), and α is the phase angle of the cutting edges ($A\hat{O}B$ angle). For the estimation of r_{CE1}, r_{CE2}, and α, a modified version of the procedure proposed in reference [12] was utilised. The tool run-out model assumes that:

- the spindle error is neglected;
- there is no inclination between the tool and the spindle axes (tilt effects are negligible).

The nano-precision machining center (Kern Pyramid Nano) used in this study guarantees this assumption. Under this hypothesis, the resolution of the geometrical problem [12] allows to derive the values of r_{CE1}, r_{CE2}, and α from the measurements of the major cutting edge radius (r_{CE1}), of the tool diameter ($\overline{AB}$ in Fig. 4a) and of the cutting force. The major cutting edge radius and the tool diameter can be measured by a microscope, while the cutting force can be measured using a load cell.

The phase α can be measured indirectly from force signals. In fact, the change of cutting edge phase from π to α causes a different cutting time between the two flutes. Referring to Fig. 4c, where an example of cutting force signal for a two-flute micro end mill with tool run-out is reported, the cutting time of the first cutting edge (T_{CE1}) is higher than that of the second cutting edge (T_{CE2}).

Table 2 Johnson-Cook model constants [25]

A	B	C	n	m
112	505	0.009	0.42	1.68

Table 3 Equation sets representing the arch-shaped curve without (Eq. (2)) and with (Eq. (3)) tool run-out

Equation set Eq. (2)	Equation set Eq. (3)
$x = r \cdot \cos(\omega \cdot t)$ $y = r \cdot \sin(\omega \cdot t) + \frac{f \cdot t}{60}$	**(a)** $x_{CE1} = r_{CE1} \cdot \cos(\omega \cdot t)$ **(a)** $y_{CE1} = r_{CE1} \cdot \sin(\omega \cdot t) + \frac{f \cdot t}{60}$ **(b)** $x_{CE2} = r_{CE2} \cdot \cos(\omega \cdot t + \alpha)$ **(b)** $y_{CE2} = r_{CE2} \cdot \sin(\omega \cdot t + \alpha) + \frac{f \cdot t}{60}$

The cutting time of each tooth depends on the cutting-edge phase angle (α) and can be estimated by using Eq. (4) and Eq. (5):

$$T_{CE1} = T \cdot \frac{2\pi - \alpha}{2\pi} \tag{4}$$

$$T_{CE2} = T \cdot \frac{\alpha}{2\pi} \tag{5}$$

where $T = T_{CE1} + T_{CE2}$ is the total cutting period. To estimate the periods (i.e., T, T_{CE1}, and T_{CE2}), a Matlab script was developed. The filtered F_x experimental force signal was fit by means of a Fourier series utilizing the Curve Fitting application of Matlab®. Once defined the fitting curve coefficients, utilizing the Matlab function "fminbnd", it is possible to locate the minima of this curve which correspond to the valleys of the force signal. In this manner, the periods T, T_{CE1}, and T_{CE2} are identified and the corresponding values of α can be calculated by using Eq. (5). More details on the procedure are reported in reference [12]. Cutting times and phase angles estimated for each test applying the above procedure are given in Table 4.

The radius of first cutting edge (r_{CE1}) can be in theory directly measured as the half of the channel width on the workpiece. The uncertainty of the measurement at this scale, high elastic recovery effects of CuZn37 brass, and the burr formation do not allow applying the previous assumption. For this reason, a new parameter namely Δr (i.e., the increment of tool radius due to tool run-out) was introduced. Once Δr value is defined, it is possible to calculate the radius of first cutting edge (r_{CE1}) by using Eq. (6):

$$r_{CE1} = \frac{\overline{AB}}{2} + \Delta rr \tag{6}$$

Table 4 Matlab estimation of the cutting time of each tooth and corresponding phase angle

	Ω [RPM]	T_{CE1} [ms]	T_{CE2} [ms]	α [°]
Test1	19,920	1.5202	1.4919	178.311
Test2	24,960	1.2180	1.1997	178.600
Test3	30,000	1.0001	0.9999	179.986

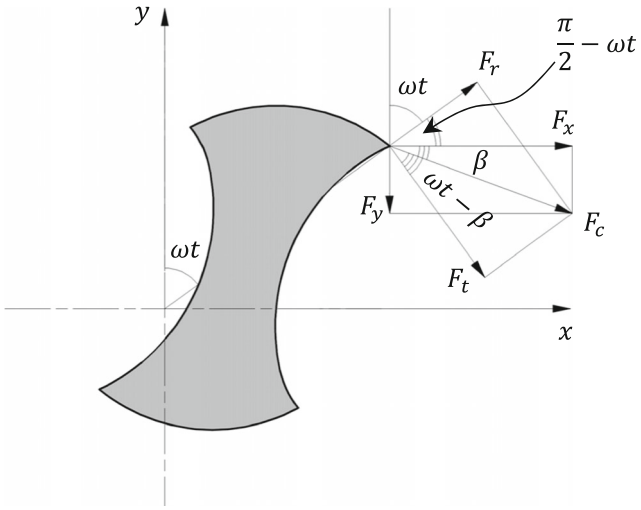

Fig. 5 Cutting force decomposition

The tool diameter ($\overline{AB}$) can be fixed at 0.782 mm (i.e., the average of the measurements). As demonstrated in reference [10], by using the law of sines on triangle AOB (Fig. 4b), β and δ are determined. Then, with the law of cosines, the radius of the second cutting edge ($r_{CE2} = \overline{OB}$) can be calculated. Finally, the tool run-out length ($r_0 = \overline{OO'}$) is determined by using the law of cosines on triangle OO'B. When all the tool run-out parameters are determined, it is possible to calculate how to offset the tool center compared to the spindle center for the FE simulation purposes.

Three different values of Δr were used in order to investigate its effect on the loads: Δr = 0.5 μm, Δr = 1 μm, and Δr = 2 μm. For each test, the best radius increment value was selected by comparing the experimental forces with an analytical prediction. The force prediction was performed using the Kronenberg model [24]. It allows calculating the tangential force component F_t as the product between the cutting pressure (K_S) and the instantaneous chip section (S), as expressed in Eq. (7):

$$F_t = S \cdot K_S \tag{7}$$

The cutting pressure depends on the instantaneous chip section. The Eq. (8) defines this relation:

$$K_S = K_{S0} \cdot S^{\left(-\frac{1}{m}\right)} \tag{8}$$

where the specific cutting pressure K_{S0} and m are the function of the tool-workpiece pair and they must be experimentally estimated. The instantaneous chip section is the product between the chip thickness and the axial depth of cut (Table 1). The chip thickness is influenced by tool run-out. It is necessary to distinguish between h_{CE1} (the instantaneous chip thickness of first cutting edge) and h_{CE2} (the instantaneous chip

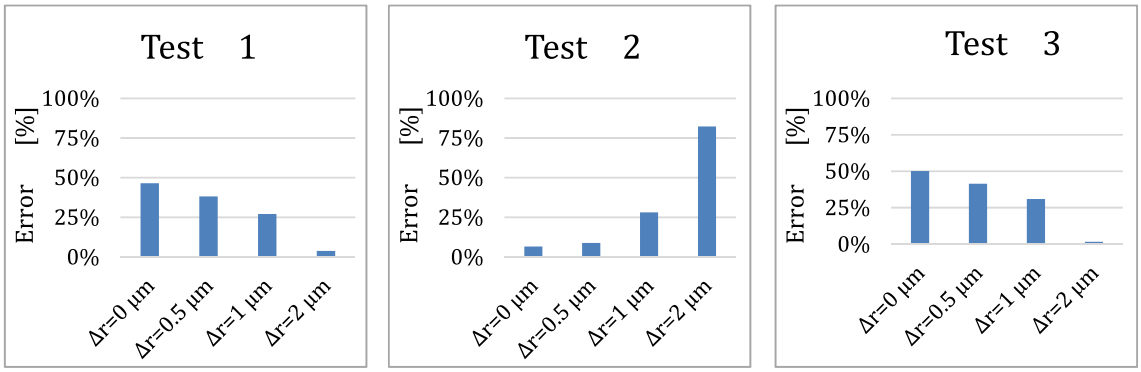

Fig. 6 The error on force predictions of the analytical model

thickness of the second cutting edge). It is possible to demonstrate (see [7]) that the different chip thicknesses can be calculated by using Eq. (9) and Eq. (10).

$$h_{CE1} = \sqrt{(r_{CE1}\sin(\omega t) + \Delta s_{CE1})^2 + (r_{CE1}\cos(\omega t))^2} - r_{CE2} \quad for\ 0 \le \omega t < \alpha \tag{9}$$

$$h_{CE2} = \sqrt{(r_{CE2}\sin(\omega t) + \Delta s_{CE2})^2 + (r_{CE2}\cos(\omega t))^2} - r_{CE1} for\ \alpha \le \omega t < 2\pi \tag{10}$$

The predicted tangential force component (F_t) must be compared with the experimental one. F_t can be calculated from the cutting force (F_c) for each time instant. As a first approximation, the geometrical model is illustrated in Fig. 5. The cutting force (F_c) can be calculated by the experimental components F_x and F_y by using Eq. (11):

$$F_c = \sqrt{F_x^2 + F_y^2} \tag{11}$$

The angle β is defined as the angle between F_c and F_x. The Eq. (12) allows calculating this angle.

$$\beta = \left|\arctan\left(\frac{F_y}{F_x}\right)\right| \tag{12}$$

The cutting force (F_c) can be decomposed in its tangential (F_t) and orthogonal (F_r) components. F_t can be obtained by Eq. (13):

$$F_t = F_c \cdot \cos(\omega t - \beta) \tag{13}$$

Once estimated the experimental tangential component (F_t) of the cutting force, a comparison with the Kronenberg prediction was done by matching the maximum values.

For each test condition, the Δr value providing the minimum error estimated according to Eq. (14) was selected as best value. Figure 6 shows the calculated errors for each test for the different Δr values.

$$Error = \left(\left| \frac{\frac{F_{t,exp,\ A}}{F_{t,exp,\ B}} - \frac{F_{t,\Delta r,\ A}}{F_{t,\Delta r,\ B}}}{\frac{F_{t,exp,\ A}}{F_{t,exp,\ B}}} \right| \right) \tag{14}$$

For test 2, the best prediction was achieved by implementing Δr = 0 μm. For test 1 and test 3, the best results are guaranteed by the maximum increment, Δr = 2 μm.

Therefore, test 2 simulation was elaborated by implementing the FE model which neglects run-out effect. Test 1 and test 3 were simulated by using the model which considers run-out effects with an increment Δr = 2 μm.

Table 5 Tool run-out parameters

Run-out parameters	Test 1	Test 2	Test 3
Tool radius [μm]	391 ± 2	391 ± 2	391 ± 2
Δr [μm]	2	0	2
r_{CE1} [μm]	393.00	391.00	393.00
r_{CE2} [μm]	389.06	391.00	389.00
r_0 [μm]	6.087	0	2.000
γ [°]	71.23	0	1.275
$\Delta x(t_1^*)$	5.734	0	0.044
$\Delta y(t_1^*)$	2.042	0	2.000
$\Delta x(t_2^*)$	− 5.792	0	− 0.045
$\Delta y(t_2^*)$	− 1.872	0	− 2.000

Table 6 Thermal and mechanical properties of materials

Properties	CuZn37	WC(Co)	(Ti,Al)N
Thermal conductivity (Ns^{-1} °C^{-1})	370	59	f(T)
Heat capacity (Nmm^{-2} °C^{-1})	3.272	15	f(T)
Thermal exp. Coeff.(°C^{-1})	2.2e-05	5e-06	9.4e-06
Young's modulus (MPa)	1.1e + 05	6.5e + 05	6.0e + 05
Poisson's ratio	0.33	0.25	0.25

Table 7 Friction modeling

Eq. (19) Sticking condition	Eq. (20) Sliding condition
$\tau_f = m \cdot k$ if $\mu \cdot p > m \cdot k$	$\tau_f = \mu \cdot p$ if $\mu \cdot p < m \cdot k$

For test 1 and test 3, the distance between O and O′ (i.e., r_0) was decomposed in x and y components, called Δx and Δy. Because of rotating tool movement, $\Delta x(t)$ and $\Delta y(t)$ change in time and can be calculated as:

$$\Delta x\,(t) = r_0 \cdot cos(k) \tag{15}$$

$$\Delta y\,(t) = r_0 \cdot sin(k) \tag{16}$$

where the time-dependent angle κ can be calculated with Eq. (17), obtained by a geometrical analysis of Fig. 4b:

$$k\,(t) = \frac{\pi}{2} - \alpha_1 - \omega t \tag{17}$$

In this equation, $\kappa(t)$ depends also on angle α_1, which can be obtained by Eq. (18).

$$\alpha_1 = \arccos\left[\frac{r_0 + \frac{AB}{2}cosy}{r_{CE1}}\right] \tag{18}$$

These results were used for both workpiece design and tool center shift compared to spindle center. Equation (3a) was used to design the workpiece profile in the simulation of the passes where the tool is engaged with r_{CE2} (tool edge B is working) and vice versa; Eq. (3b) was used when the tool was engaged with r_{CE1} (tool edge A is working).

In FE simulations without run-out, tool was positioned with its center O′ overlapped to the spindle rotation center O and then a rotation around O ≡ O′ was set. In FE simulations with tool run-out, tool center O′ was initially offset by $\Delta x(t^*)$ and $\Delta y(t^*)$, calculated at different time (t_1^* and t_2^*) for simulation of tool edge A and tool edge B: the first edge starts to engage the workpiece when $\omega t_1^* = 0$; the second edge starts to engage the workpiece when $\omega t_2^* = 2\pi - \alpha$. Then, the tool rotation was set around spindle center O, from 0° to 180°. In Table 5, the parameters of each test for the FE simulation design considering tool run-out are summarized.

As previously explained, the movement was assigned to the tool, using speeds according to the experimental values. The tool boundary conditions allow transferring heat throughout the entire body. The heat transfer conduction coefficient between tool and workpiece plays a key role in chip formation thermodynamics [15, 18]. This parameter was set equal to 10^5 N s^{-1} mm^{-1} $°C^{-1}$. It is higher than usual value, and it is necessary to generate sufficient temperature in the short duration of the simulation (about 0.001 s). The heat exchange was also allowed between the chip-tool system and the environment. All material properties for the workpiece, the tool, and the coating are given in Table 6.

The friction between workpiece and tool was modeled using the hybrid model available in DEFORM-3D, which considers both sticking and sliding contacts [15, 18] by Eq. (19) and Eq. (20) (Table 7).

In these equations, τ_f is the frictional stress, k is the shear yield stress, and p is the interface pressure. The shear friction factor m was set equal to 0.9 and the Coulomb friction coefficient μ was fixed at 0.4 [15]. The chip curvature brings a contact also between itself and the workpiece, that contact was modeled by the sliding condition with a Coulomb friction coefficient of 0.1.

4 4. Comparison of predicted cutting forces and chip shapes

It was observed that the FE simulations of micro milling achieve a good prediction of the experimental forces. For simulation without considering tool run-out, test 2 is used because the run-out was minimum in this experiment (the least tool run-out condition). In Fig. 7a, b, a comparison between simulated and experimental force results for test 2 is presented showing reasonably good agreements.

In Fig. 8, the same comparison between experimental and finite element method (FEM) results is shown for

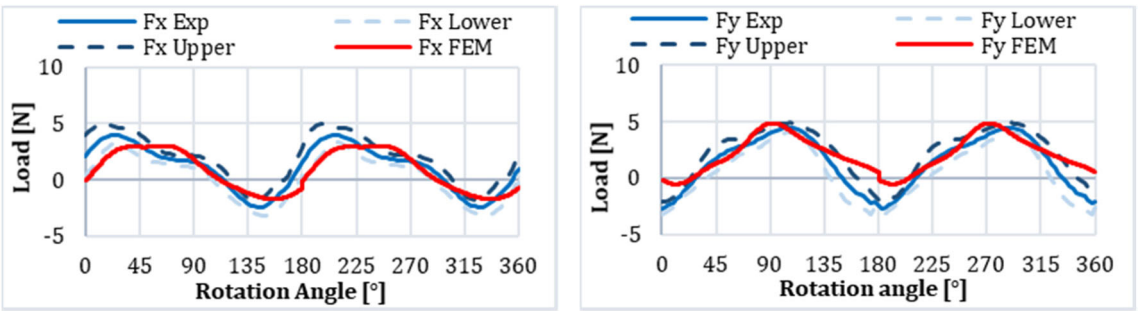

Fig. 7 Comparison of predicted and experimental forces (test 2—no tool run-out considered)

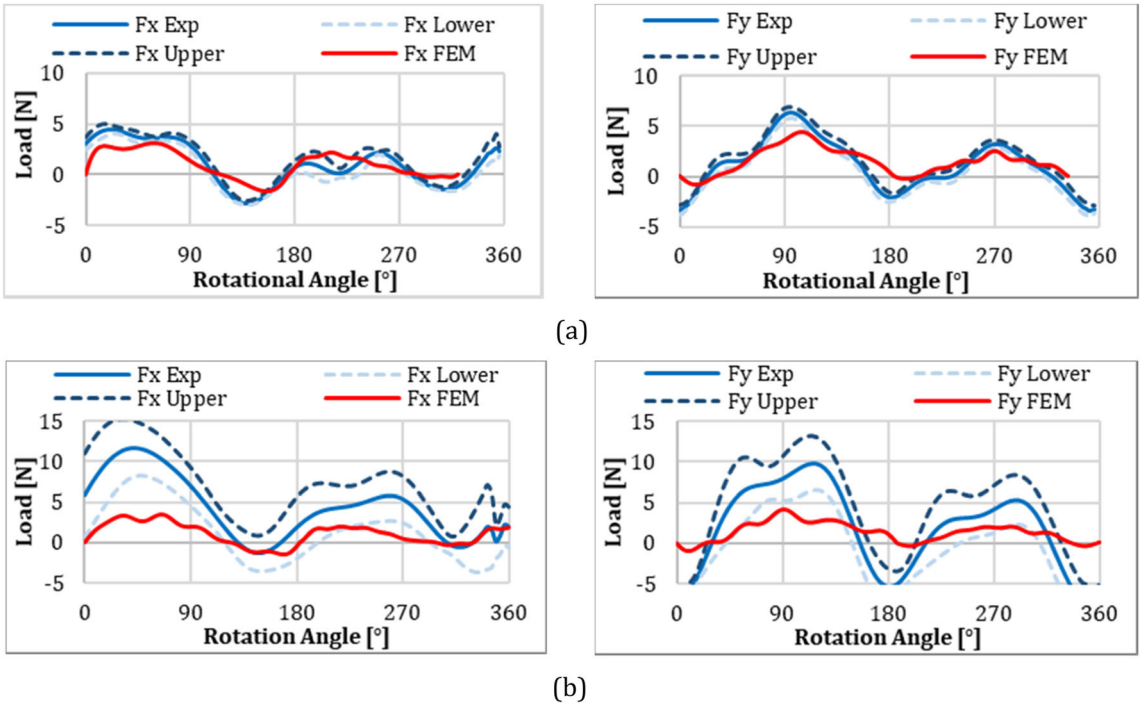

Fig. 8 Comparison of predicted and experimental forces (**a**) test 1; **b**) test 3 (tool run-out considered)

test 1 (Fig. 8a) and test 3 (Fig. 8b) considering tool run-out due to a value of Δr equal to 2 μm. It is evident that the model validity for test 3 is not satisfactory. Experimental loads for this test are significantly higher than the force values of test 1 and test 2. A possible explanation for this can be related to the experimental set-up. The thin-wall cut with higher cutting speed undergoes to greater vibrations which affect the force measurements. Furthermore, considering the simulation results, it is well-known how, at the high cutting speed (i.e., higher strain rates), the material constitutive law expressed by the Johnson-Cook model underestimates the actual flow stresses and, as a consequence, the predicted cutting forces.

In addition, reasonably good results are obtained for the chip shapes from the FE simulations. Figure 9 shows the comparison between simulated and experimental chip shapes for test 2. It is possible to observe that the simulation is able to predict the some chip segmentation as well.

Simulated chip body also shows significant effective strain but a low temperature as shown in Fig. 10 shows indicating that plastic deformation is large but heat generated in this micro milling process with such small feed per tooth values is not very high (around 50 °C).

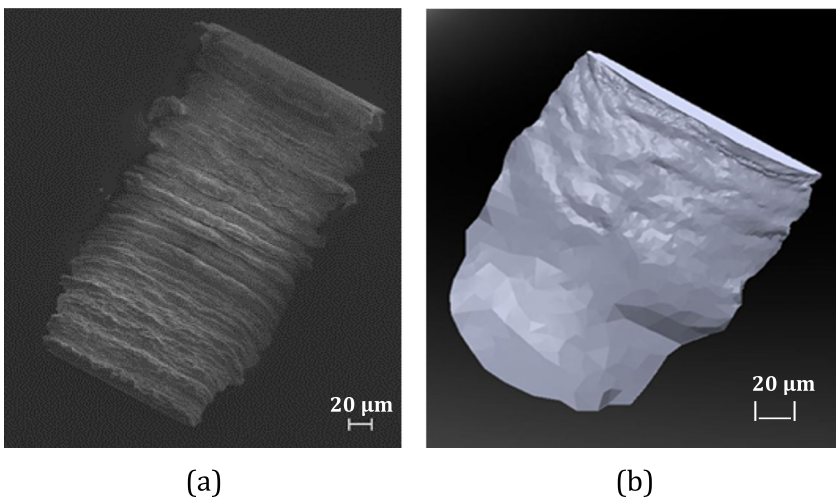

Fig. 9 The comparison between a SEM image of a chip sample (**a**) and a part of the simulated chip shape (**b**) for test 2

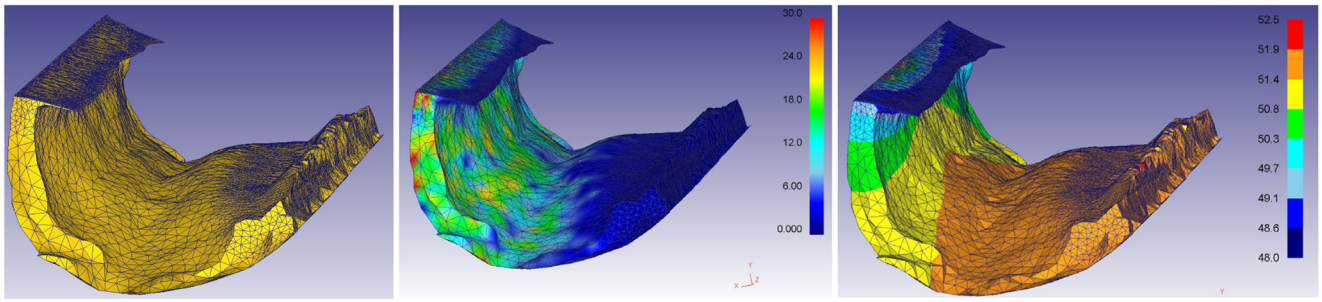

Fig. 10 **a** Simulated chip geometry with deformed mesh, **b** predicted effective strain distribution, and **c** predicted temperature distribution in °C

5 Conclusions

This study presents an experimental and finite element simulation-based investigations about the effect of tool run-out on 3D orthogonal micro milling configuration. The size of the tool run-out deviation does not result in direct connection to the cutting speed and it remains in the magnitude order of few micrometres. The cutting forces are significantly influenced by tool run-out and this effect can be reliably predicted by the FE simulation model coupled with tool run-out. This methodology relies on measurement of tool run-out from orthogonal micro-milling tests and on measuring cutting forces generated by two flutes of the micro end mill. It was shown that while FE simulations accurately predict cutting forces in the presence of no tool run-out effect, the improved FE simulation methodology by considering tool motion with calculated tool run-out results in reasonably good cutting force predictions as well. It is also noted that the qualitative comparison of predicted chip flow and chip shapes and the measured chip shapes yields in reasonably good results. A more quantitative analysis of experimental chip samples as compared with predicted chips is required for further validating the mechanism of chip formation when considering tool run-out in micro milling processes.

References

1. Dornfeld D, Mina S, Takeuchi Y (2006) Recent advances in mechanical micromachining. CIRP Ann Manuf Technol 55:745–768
2. Cheng K, Huo D (2013) Micro cutting: fundamentals and applications. John Wiley & Sons, Chichester
3. Bissacco G, Hansen HN, Slunsky J (2008) Modelling the cutting edge radius size effect for force prediction in micro milling. CIRP Ann Manuf Technol 57:113–116
4. Özel T, Bartolo P, Ceretti E, Ciurana J, Rodriguez CA, Lopes Da Silva JV (2016) Biomedical devices: design, prototyping and manufacturing. Wiley, Hoboken
5. Karagiannis S, Stavropoulos P, Ziogas C, Kechagias J (2013) Prediction of surface roughness magnitude in computer numerical controlled end milling processes using neural networks, by considering a set of influence parameters: an Aluminium alloy 5083 case study. Proc Inst Mech Eng B J Eng Manuf 228(2):233–244
6. Annoni M, Pusterla N, Rebaioli L, Semeraro Q (2015) Calibration and validation of a mechanistic micromilling force prediction model. J Manuf Sci Eng 138:11001–11012
7. Attanasio A, Garbellini A, Ceretti E, Giardini C (2015) Force modelling in micromilling of channels. Int J Nanomanuf 11(5–6): 275–296
8. Gelfi M, Attanasio A, Ceretti E, Garbellini A, Pola A (2015) Micromilling of lamellar Ti6Al4V: cutting force analysis. Mater Manuf Process 31(7):919–925
9. Riviere-Lorphevre E, Letot C, Ducobu F, Dehombreux P, Filippi E (2017) Dynamic simulation of milling operations with small diameter milling cutters: effect of material heterogeneity on the cutting force model. Meccanica 52:35–44
10. Wang JJ, Uhlmann E, Oberschmidt D, Sung CF, Perfilov I (2016) Critical depth of cut and asymptotic spindle speed for chatter in micro milling with process damping. CIRP Ann Manuf Technol 65(1):113–116
11. Uhlmann E, Oberschmidt D, Kuche Y, Löwenstein A (2014) Cutting edge preparation of micro milling tools. Procedia CIRP 14:349–354
12. Attanasio A (2017) Tool run-out measurement in micro milling. Micromachines 8:221
13. Davoudinejad A, Tosello G, Parenti P, Annoni M (2017) 3D finite element simulation of micro end-milling by considering the effect of tool run-out. Micromachines 8(187):1–20
14. Mamedov A, Lazoglu I (2016) Thermal analysis of micro milling titanium alloy Ti-6Al-4V. J Mater Process Technol 229:659–667
15. Thepsonthi T, Özel T (2015) 3-D finite element process simulation of micro-end milling Ti-6Al-4V titanium alloy: experimental validations on Chip flow and tool Wear. J Mater Process Technol 221: 128–145
16. Thepsonthi T, Özel T (2016) Simulation of serrated chip formation in micro-milling of titanium alloy Ti-6Al-4V using 2D elasto-viscoplastic finite element modeling. Prod Eng Res Dev 10(6): 575–586
17. Ucun I, Aslantas K, Bedir F (2016) Finite element modeling of micro-milling: numerical simulation and experimental validation. Mach Sci Technol 20(1):148–172

18. Özel T, Olleak A, Thepsonthi T (2017) Micro milling of titanium alloy Ti-6Al-4V: 3-D finite element modeling for prediction of chip flow and burr formation. Prod Eng 11(4–5):435–444
19. Biermann D, Kahnis P (2010) Analysis and simulation of size effects in micromilling. Product Eng Res Dev 4(1):25–34
20. Park SS, Malekian M (2009) Mechanistic modeling and accurate measurement of micro end milling forces. CIRP Ann Manuf Technol 58:49–52
21. Malekian M, Park SS, Jun MBG (2009) Modeling of dynamic micro-milling cutting forces. Int J Mach Tools Manuf 49:586–598
22. Altintas Y, Jin X (2011) Mechanics of micro-milling with round edge tools. CIRP Ann Manuf Technol 60(1):77–80
23. Korkmaz E, Gozen BA Bediz B, Ozdoganlar OB (2017) Accurate measurement of micromachining forces through dynamic compensation of dynamometers. Precis Eng 49:365–376
24. Kronenberg M (1966) Machining science and application. Pergamon Press
25. Johnson GJ, Cook WH (1983) A constitutive model and data for metals subjected tool large strains, high strain rates and high temperatures. Proc 7th international Symposium on Ballistics 541–547